

Memory-Scalable and Hardware-Adaptive Matrix-Free Quantum Simulation

Uriel Shafir and Ronnie Kosloff

The Institute of Chemistry, The Hebrew University of Jerusalem, Jerusalem 9190401, Israel

(Dated: 1 July 2026)

The core step in quantum simulations is typically matrix vector multiplication $\phi = \hat{H}\psi$. Executing this step is limited by memory requirement to store the Hamiltonian. We present a memory-scalable, hardware-adaptive matrix-free framework for applying large operators on vectors without materializing the full matrix on a single accelerator.

The operator is represented through a block-procedural interface: blocks may be generated, loaded, cached, distributed, or applied directly only when their action is needed. For quantum simulation, it provides the core kernel for quantum operations. An adaptive planner selects block size, cache strategy, GPU grouping, row distribution, and task parallelization from memory and workload estimates. We describe analytic, measured, and learned planning strategies that choose between procedural generation, partial caching, full caching, and row-distributed caching. The method removes the requirement that the full dense matrix fit in the accelerator memory. This shifts large simulations from a fixed memory barrier to a tunable balance between block generation, cache reuse, data movement, parallel scheduling, and numerical accuracy.

I. INTRODUCTION

Exact and near-exact numerical quantum simulations play an important role in modern quantum science and engineering. They are used to benchmark quantum devices, validate quantum algorithms, study many-body dynamics, test approximations, and provide reference calculations for quantum technologies¹. As quantum hardware improves, simulation on classical hardware maintains its importance; rather, the need for larger and more reliable reference simulations becomes more acute.

At the computational level, the method developed in this work addresses a more general primitive: the application of a large linear operator or matrix to a vector,

$$\vec{y} = \mathbf{A}\vec{x}, \quad (1)$$

where ($A \in \mathbb{C}^{M \times D}$), ($x \in \mathbb{C}^D$) and ($y \in \mathbb{C}^M$). The matrix (\mathbf{A}) need not be square. Thus, the same block-procedural and matrix-free ideas apply to general rectangular matrix-vector products, linear maps, filters, projections, embeddings, super-operators, and other large-scale linear transformations. The central requirement is not that (\mathbf{A}) be a Hamiltonian, but that the action ($\mathbf{A}\vec{x}$) can be evaluated from blocks, generated entries, cached pieces, or fused local actions without explicitly storing the full matrix.

Quantum numerical simulation provides a prominent and physically important special case. Taking ($\mathbf{A} = \hat{H}$), ($\vec{x} = \psi$), and ($\vec{y} = \phi$) defines the Hamiltonian-vector product

$$\phi = \hat{H}\psi. \quad (2)$$

This operation appears is the basic step in any polynomial approximation of a function of $f(\hat{H})$ ². For example a Chebychev polynomial expansion of the real-time propagation $e^{-i\hat{H}t}$ ³, imaginary-time filtering⁴⁻⁶, Krylov methods⁷, Green functions⁸ and more⁹. Typically in these quantum-simulation algorithms, repeated application of \hat{H} is the dominant computational kernel¹⁰.

Although the discussion in this paper is framed around quantum simulation, the same computational strategy is relevant

beyond quantum mechanics^{9,11-14}. Many large-scale problems in scientific computing and artificial intelligence are dominated by repeated applications of large linear maps, often too large to store or move efficiently in explicit dense form. Matrix-free, block-generated, cached, and hardware-adaptive matrix-vector multiplication can therefore be useful wherever the main bottleneck is the application of a large matrix or operator rather than the formal definition of the matrix itself¹⁵.

If the Hilbert-space dimension is D , explicit storage of a dense Hamiltonian requires $O(D^2)$ complex numbers. This quadratic storage cost is the matrix-size problem addressed in this work. The vector itself has only linear size $O(D)$. Although vector storage can also be important in very large simulations, it is not the focus of the present framework. Here we focus on avoiding the need to materialize the full $D \times D$ Hamiltonian matrix on one accelerator.

The Hamiltonian is not stored as a global matrix. Instead, it is represented by a procedural interface that can produce dense block entries, or their action, when they are needed. The global Hamiltonian remains a well-defined matrix, but the computation never requires materializing it as a full $D \times D$ object on one device.

The framework is general and can be applied to Hamiltonians whose blocks are generated from reproducible random seeds, reconstructed from analytic formulas, loaded from host memory or external storage, retrieved from a database, or evaluated through a fused action. These sources are treated uniformly by the matrix-free interface. The important requirement is that, for each pair of block indices (n, m) , the framework can obtain the block $\hat{H}^{[n,m]}$ or compute the product $\hat{H}^{[n,m]}\psi^{[m]}$ directly.

A fixed block representation is still not enough. The efficient choice of block size, caching strategy, data layout, and parallelization depends on the hardware. A calculation that is best served by full matrix caching on a large-memory GPU may require row-distributed full caching, partial caching, or procedural generation on a smaller system. A scan over coupling strengths may parallelize naturally over parameter values, while a single large application may require splitting the output

block rows across multiple GPUs¹⁶. We therefore include a hardware-adaptive execution layer as part of the method.

The examples in this paper focus on two broad tasks. First, we describe propagation using polynomial, Krylov, or stepwise integrators whose dominant kernel is repeated application of \hat{H} . Second, we describe stochastic thermal pure quantum calculations, in which a thermal state is represented by a filtered random vector and observables are estimated from one or more typical pure states¹⁷. In both cases, the computational engine is the same blockwise matrix-free Hamiltonian-vector product.

The paper is organized as follows. Section II defines the block representation. Section III presents the procedural matrix-free matrix-vector product. Section IV describes hardware-adaptive execution planning, including analytic, measured, and learned plan-selection algorithms. Section V analyzes matrix-storage and runtime scaling. Section VI discusses GPU-resident caching and row distribution. Section VII presents propagation use cases. Section VIII discusses limitations and design implications. Section IX concludes with scope, extensions, and limitations.

II. HAMILTONIAN BLOCK REPRESENTATION

Let \mathcal{H} be a finite-dimensional Hilbert space of dimension D . A quantum state in this Hilbert space is represented by a vector

$$\psi \in \mathbb{C}^D,$$

and the Hamiltonian is represented by a linear operator

$$\hat{H} : \mathbb{C}^D \rightarrow \mathbb{C}^D.$$

In a standard dense-matrix representation, \hat{H} would be stored as a $D \times D$ complex matrix. For large D , this representation is usually impossible on a single GPU because the memory required to store \hat{H} scales as D^2 . The purpose of the block representation introduced here is not to change the mathematical Hamiltonian, but to group its matrix elements and vector components in a way that is useful for computation.

We partition the full vector space into N_{blk} computational blocks. The size of block n is denoted by b_n , so that

$$D = \sum_{n=0}^{N_{\text{blk}}-1} b_n.$$

Here N_{blk} is the number of blocks, while b_n is the number of vector components stored in the n -th block. The blocks may all have the same size, but this is not required. The partition is a computational device: it does not necessarily correspond to a physical decomposition into subsystems, lattice sites, energy sectors, symmetry sectors, or system-bath components. Such interpretations may exist in specific applications, but they are not assumed by the framework.

The block number N_{blk} should therefore be understood as an execution parameter, not as a physical parameter. Changing N_{blk} changes how the matrix is partitioned, but should not change the mathematical operator being applied. In seeded or

procedural implementations this requires care: if the random generator is indexed by block labels rather than by global matrix indices, then changing the block partition can produce a different random Hamiltonian realization. A partition-invariant implementation should generate matrix elements, or deterministic block entries, from global row and column indices. Otherwise, N_{blk} becomes part of the ensemble definition rather than a purely computational choice.

With this partition, the state vector is written as

$$\psi = \begin{pmatrix} \psi^{[0]} \\ \psi^{[1]} \\ \vdots \\ \psi^{[N_{\text{blk}}-1]} \end{pmatrix}, \quad \psi^{[n]} \in \mathbb{C}^{b_n}.$$

The notation $\psi^{[n]}$ denotes the n -th block of the state vector. If α labels a component inside block n , then

$$\psi_{\alpha}^{[n]}, \quad \alpha = 0, \dots, b_n - 1,$$

denotes the α -th component of the n -th block. The pair (n, α) therefore labels one component of the original global vector ψ .

The Hamiltonian is partitioned in the corresponding way. It is written as a block matrix

$$\hat{H} = \begin{pmatrix} \hat{H}^{[0,0]} & \hat{H}^{[0,1]} & \dots & \hat{H}^{[0,N_{\text{blk}}-1]} \\ \hat{H}^{[1,0]} & \hat{H}^{[1,1]} & \dots & \hat{H}^{[1,N_{\text{blk}}-1]} \\ \vdots & \vdots & \ddots & \vdots \\ \hat{H}^{[N_{\text{blk}}-1,0]} & \hat{H}^{[N_{\text{blk}}-1,1]} & \dots & \hat{H}^{[N_{\text{blk}}-1,N_{\text{blk}}-1]} \end{pmatrix}. \quad (3)$$

The block $\hat{H}^{[n,m]}$ maps input block m of the vector into output block n . Therefore,

$$\hat{H}^{[n,m]} \in \mathbb{C}^{b_n \times b_m}.$$

The first index n refers to the output block, and the second index m refers to the input block. In component notation,

$$\hat{H}_{\alpha\beta}^{[n,m]}$$

is the matrix element that couples component β of input block m to component α of output block n .

It is important to emphasize that Eq. (3) is completely general. Every finite-dimensional Hamiltonian can be written in this form after choosing a partition of the vector components. The block representation does not imply that the Hamiltonian is block diagonal. It also does not imply that most blocks are zero. In the most general case, every block $\hat{H}^{[n,m]}$ may be dense and nonzero. Thus, the framework allows the Hamiltonian to be fully dense at the global level, even though the notation groups the matrix entries into blocks.

The action of the Hamiltonian on a state vector is

$$\phi = \hat{H}\psi,$$

where $\phi \in \mathbb{C}^D$ is the output vector. After partitioning ϕ in the same way as ψ ,

$$\phi = \begin{pmatrix} \phi^{[0]} \\ \phi^{[1]} \\ \vdots \\ \phi^{[N_{\text{blk}}-1]} \end{pmatrix}, \quad \phi^{[n]} \in \mathbb{C}^{b_n},$$

the matrix-vector product becomes

$$\phi^{[n]} = \sum_{m=0}^{N_{\text{blk}}-1} \hat{H}^{[n,m]} \psi^{[m]}. \quad (4)$$

In component form,

$$\phi_{\alpha}^{[n]} = \sum_{m=0}^{N_{\text{blk}}-1} \sum_{\beta=0}^{b_m-1} \hat{H}_{\alpha\beta}^{[n,m]} \psi_{\beta}^{[m]}, \quad \alpha = 0, \dots, b_n - 1. \quad (5)$$

This expression is the ordinary dense matrix-vector product written with two levels of indexing: a block index and an index inside each block.

For clarity, consider the special case in which all blocks have the same size,

$$b_n = b, \quad D = N_{\text{blk}} b.$$

Then every block $\hat{H}^{[n,m]}$ is a $b \times b$ matrix, and the full Hamiltonian contains N_{blk}^2 such blocks. If all blocks are dense and nonzero, storing all of them is equivalent to storing a dense $D \times D$ Hamiltonian. Therefore, the block notation by itself does not reduce the number of mathematical matrix elements. It only specifies how the entries of the Hamiltonian and the components of the vector are grouped.

No approximation has been introduced by this notation. The Hamiltonian remains the full operator \hat{H} , and the block decomposition only specifies how its matrix elements are indexed. The computational advantage comes in the next step: instead of assembling all blocks at once, the matrix-vector product can be evaluated by generating, loading, caching, or applying only the blocks required for the current part of the computation.

III. PROCEDURAL MATRIX-FREE MATRIX-VECTOR MULTIPLICATION

The block representation of Sec. II is useful because it allows the product

$$\phi = \hat{H} \psi$$

to be evaluated without assembling the full $D \times D$ Hamiltonian in GPU memory. Section II defined the mathematical object. This section describes the computational procedure used to apply that object.

For a single pair of block indices (n, m) , we represent this operation abstractly as

$$\text{apply_H_block}(n, m, \psi^{[m]}) = \mathcal{G}(n, m; \Theta_{n,m}) \psi^{[m]}. \quad (6)$$

Here $\mathcal{G}(n, m; \Theta_{n,m})$ denotes the procedural representation of the Hamiltonian block $\hat{H}^{[n,m]}$. The symbol $\Theta_{n,m}$ denotes the data required to define that block. Depending on the implementation, $\Theta_{n,m}$ may contain a random seed, parameters of an analytic formula, a database key, a file offset, compression metadata, cached block data, or other information needed to reconstruct or apply the block.

Equation (6) is an interface, not necessarily an instruction to explicitly build the block as a dense array. In the most direct implementation, the block $\hat{H}^{[n,m]}$ is generated or loaded as a dense array, multiplied by $\psi^{[m]}$, and then released. More memory-restricted implementations may compute the same block action in smaller internal pieces, or may fuse block generation with the contraction. The external operation remains the block product $\hat{H}^{[n,m]} \psi^{[m]}$.

With this interface, the complete output block is

$$\phi^{[n]} = \sum_{m=0}^{N_{\text{blk}}-1} \text{apply_H_block}(n, m, \psi^{[m]}). \quad (7)$$

Thus, the full matrix-vector product can be interpreted as a loop over output blocks n , where each output block is formed by a loop over input blocks m . The global Hamiltonian is never materialized. Instead, the algorithm evaluates block contributions and accumulates them into the output vector.

A. Sources and storage modes for block data

The same matrix-free interface supports several modes of specifying and storing Hamiltonian blocks.

a. Seeded generation. A block may be generated reproducibly from a seed:

$$\hat{H}^{[n,m]} = \mathcal{G}_{\text{seed}}(n, m, s_{n,m}). \quad (8)$$

The stored object is the seed $s_{n,m}$ and the generation rule, not the dense matrix itself. This is useful for random-matrix benchmarks, stochastic environments, or controlled ensembles of Hamiltonians.

b. Analytic generation. A block may be defined by a formula

$$\hat{H}_{\alpha\beta}^{[n,m]} = f(n, m, \alpha, \beta; \theta). \quad (9)$$

The matrix entries are computed when needed. In this case the Hamiltonian is defined by the function f and the parameter set θ , rather than by a stored dense array.

c. Externally stored blocks. A block may be stored outside GPU memory and retrieved by key:

$$\hat{H}^{[n,m]} = \mathcal{D}[\text{key}(n, m)]. \quad (10)$$

The external storage can contain complete dense blocks, compressed representations, deterministic model records, calibrated experimental blocks, or learned matrix surrogates. The computational kernel remains unchanged: the block is loaded or reconstructed only for the currently active part of the matrix-vector product.

d. Fused action. The most memory-efficient implementation may expose only the action

$$\psi^{[m]} \mapsto \hat{H}^{[n,m]} \psi^{[m]} \quad (11)$$

without ever forming $\hat{H}^{[n,m]}$ as a dense array. This is still the same Hamiltonian-vector product and can be used by any algorithm that requires only applications of \hat{H} .

e. Full caching. If memory permits, all required blocks can be stored on the GPU. This removes repeated generation or loading costs and is advantageous when the same Hamiltonian is applied many times, as in Krylov, Chebyshev, and TPQ calculations.

f. Partial caching. If full caching does not fit in memory, a fixed memory budget can be used to cache only a subset of blocks. Cached blocks are reused directly, while uncached blocks are generated or loaded on demand. For Hermitian operators, it is natural to cache canonical block pairs (n, m) with $n \leq m$, using

$$\hat{H}^{[m,n]} = \left(\hat{H}^{[n,m]} \right)^\dagger.$$

Partial caching interpolates between full procedural regeneration and full matrix caching.

B. Block-row accumulation

For dense Hamiltonians, every output block generally receives contributions from every input block. The exact deterministic product therefore includes all block pairs. The calculation may still be scheduled by output block rows: a GPU or GPU group can own a subset of output blocks and accumulate

$$\phi^{[n]} = \sum_{m=0}^{N_{\text{blk}}-1} \hat{H}^{[n,m]} \psi^{[m]}, \quad n \in \mathcal{R},$$

where \mathcal{R} is the assigned row set. This scheduling changes the memory layout and the parallel work distribution, but it does not change the Hamiltonian or omit any block products.

A reference pseudocode implementation is:

```

for R_out in output_block_row_groups:
    phi_R = zeros_for_output_rows(R_out)
    for n in R_out:
        for m in range(N_blk):
            H_nm = generate_load_or_fetch_cached_block(n,
                m)
            phi_R[n] += apply_block(H_nm, psi[m])
    save_or_return_output_rows(R_out, phi_R)

```

For an exact dense calculation, all input-block indices m are included for each output row n . If the block graph is known to be sparse, the loop over m can be restricted to the nonzero block neighbors. Such a restriction is exact only when the omitted blocks are truly zero; otherwise it defines a truncated or stochastic approximation.

IV. HARDWARE-ADAPTIVE EXECUTION PLANNING

The block representation defines how the mathematical operator can be applied. An efficient implementation must also decide how the work should be scheduled on the available hardware. We therefore introduce an adaptive execution plan. The plan is a set of choices made before a run, or before each problem size in a sweep, based on device memory, number of GPUs, expected arithmetic work, and user accuracy requirements.

An execution plan may include:

- the block count N_{blk} and block sizes b_n ;
- the matrix storage mode: procedural, full-cache, partial-cache, or externally loaded;
- the cache budget per GPU;
- the number of cached Hermitian block pairs;
- the GPU grouping strategy;
- whether work is distributed over independent parameter values, output block rows, or both;
- a safety estimate for dense arithmetic work;
- spectral and sampling parameters used by propagation or correlation routines.

A. Generic dense matrix–multi-vector planning problem

The execution planner is not tied to a Hamiltonian. Its generic computational object is a dense matrix–multi-vector product

$$Y = AX, \quad A \in \mathbb{C}^{D_{\text{out}} \times D_{\text{in}}}, \quad X \in \mathbb{C}^{D_{\text{in}} \times R}, \quad Y \in \mathbb{C}^{D_{\text{out}} \times R}. \quad (12)$$

Here R denotes the number of vectors to which the same matrix is applied simultaneously. The ordinary matrix-vector case corresponds to $R=1$. A block Hamiltonian application in a tensor-product system–bath model can be viewed as a dense bath operator acting on $R = d_S$ simultaneous state components, one for each system degree of freedom.

For n_{op} dense operators applied in one kernel evaluation, the leading arithmetic scale is

$$F_{\text{mv}} \approx 8 n_{\text{op}} D_{\text{out}} D_{\text{in}} R, \quad (13)$$

where the factor 8 is the usual real-operation count scale for one complex multiply-add. The square Hamiltonian-vector case is recovered by setting $D_{\text{out}} = D_{\text{in}} = D$ and $R = 1$, giving $F_{\text{mv}} \sim 8D^2$. For the kicked TPQ/HMF application considered below, the dense bath-side operators have

$$D_{\text{out}} = D_{\text{in}} = d_B, \quad R = d_S, \quad n_{\text{op}} = 1 + n_{\text{int}},$$

where the first operator is the bath Hamiltonian and the remaining operators come from the interaction terms.

A generic planning instance is therefore specified by

$$\mathcal{P}_{mv} = (D_{\text{out}}, D_{\text{in}}, R, n_{\text{op}}, N_{\text{task}}, B_c, M_{\text{free}}, N_{\text{GPU}}),$$

D_{out}	number of output rows of the dense linear map,
D_{in}	number of input rows, or columns of the dense map,
R	number of simultaneous vectors multiplied by the same operator,
n_{op}	number of dense operators applied per kernel call,
N_{task}	number of independent outer-loop tasks,
B_c	bytes per complex scalar,
M_{free}	available accelerator memory,
N_{GPU}	number of available accelerators.

Thus D_{out} and D_{in} specify the shape of the matrix, R specifies how many vectors are multiplied at once, and n_{op} specifies how many dense matrix actions are fused into one planned operation. The task count N_{task} counts independent outer-loop jobs, such as coupling values, disorder realizations, temperatures, probe vectors, or independent data batches. The scalar B_c is usually 8 bytes for single-precision complex arithmetic and 16 bytes for double-precision complex arithmetic. For a multi-GPU node, M_{free} should be interpreted as the vector

$$M_{\text{free}} = (M_{\text{free}}^{(1)}, \dots, M_{\text{free}}^{(N_{\text{GPU}})}),$$

and the conservative memory tests below use its smallest component. The planner chooses a block partition, storage mode, cache budget, row-group size, and distribution of tasks over GPU groups.

B. Memory-constrained cost-model planner

The first optimizer is an analytic planner. It enumerates feasible candidate plans and rejects plans that cannot satisfy a memory safety constraint. If the algorithm keeps r temporary arrays of size $D_{\text{in}} \times R$ in accelerator memory, the workspace memory is estimated as

$$M_{\text{work}} = r D_{\text{in}} R B_c. \quad (14)$$

For full caching of n_{op} dense matrices over a row group of size p_{row} , the per-GPU matrix memory is approximately

$$M_{\text{full}} = \frac{n_{\text{op}} D_{\text{out}} D_{\text{in}} B_c}{p_{\text{row}}}. \quad (15)$$

For a square Hermitian block representation with equal block size b , a partial cache containing P_{cache} canonical block pairs per operator costs

$$M_{\text{partial}} = n_{\text{op}} P_{\text{cache}} b^2 B_c. \quad (16)$$

The total estimated per-GPU memory is

$$M_{\text{tot}} = M_{\text{op}} + M_{\text{work}}, \quad M_{\text{op}} \in \{0, M_{\text{partial}}, M_{\text{full}}\}, \quad (17)$$

and a plan is accepted only if

$$M_{\text{tot}} \leq \alpha \min_j M_{\text{free}}^{(j)}, \quad (18)$$

where $0 < \alpha < 1$ is a safety fraction.

Among the memory-feasible candidates, the analytic planner assigns a rough runtime score. Let $C(p)$ be the number of GPU groups that can work on independent tasks under plan p . The number of task waves is

$$W(p) = \left\lceil \frac{N_{\text{task}}}{C(p)} \right\rceil. \quad (19)$$

The cost-model score is then

$$S_{\text{model}}(p) = W(p) \frac{F_{\text{mv}}}{R_{\text{eff}}(p)} \Pi_{\text{cache}}(p) \Pi_{\text{mem}}(p), \quad (20)$$

where $R_{\text{eff}}(p)$ is an effective throughput estimate, Π_{cache} penalizes procedural regeneration or incomplete caching, and Π_{mem} penalizes operation close to the memory limit. This score is used only to rank and prune candidates; measured autotuning, when enabled, overrides it.

a. Algorithm 1: analytic memory-constrained planning. Given \mathcal{P}_{mv} , enumerate candidate block counts, operator-storage modes, row-group sizes, and task-grouping modes. For each candidate p , compute M_{work} , M_{op} , and M_{tot} . Reject p if Eq. (18) fails. For each surviving plan, compute $S_{\text{model}}(p)$ from Eq. (20). The analytic plan is

$$p_{\text{model}} = \arg \min_p S_{\text{model}}(p).$$

C. Measured Microbenchmark Autotuning

The second optimizer is a measured autotuner. The analytic planner described above is useful for rejecting plans that cannot fit in memory. However, it cannot predict the actual runtime accurately in all cases. The real runtime depends on hardware details such as GPU model, memory bandwidth, FP32 or FP64 throughput, cache behavior, communication, kernel launch overhead, and the cost of generating matrix blocks procedurally.

Therefore, after the analytic planner has produced a small set of feasible candidate plans, the measured autotuner tests these plans directly on the available hardware. Each candidate plan is run using the same matrix-free kernel that will be used in the full production calculation. The purpose of this stage is simple: instead of guessing which feasible plan is fastest, the code measures it.

Let p denote one candidate execution plan. A plan p includes choices such as the block size, cache mode, row-group size, GPU grouping, and whether the calculation is distributed over parameter values, output block rows, or a hybrid of both.

Before timing the candidate plan, the autotuner performs R_{warm} warmup applications. These warmup applications are not included in the timing. They are used to remove one-time overheads such as GPU initialization, memory allocation, cache setup, and kernel compilation.

After the warmup stage, the autotuner performs R_{bench} timed applications of a representative matrix-free operation. In this context, a representative operation means one application of the same type of matrix-vector or matrix-multi-vector product

that appears in the full calculation. It has the same matrix dimensions, block structure, block source, cache strategy, and GPU distribution as the candidate plan being tested.

If $t_q(p)$ is the measured time of the q -th timed application under plan p , then the average measured time per matrix-free application is

$$\widehat{t}_{\text{mv}}(p) = \frac{1}{R_{\text{bench}}} \sum_{q=1}^{R_{\text{bench}}} t_q(p). \quad (21)$$

Here:

- p is the candidate execution plan being tested.
- R_{warm} is the number of warmup applications.
- R_{bench} is the number of timed benchmark applications.
- q labels one timed benchmark repetition.
- $t_q(p)$ is the measured time of benchmark repetition q using plan p .
- $\widehat{t}_{\text{mv}}(p)$ is the average measured time for one matrix-vector or matrix-multi-vector application using plan p .

The fastest single matrix-vector application is not always the fastest full job. Some plans use all GPUs together for one task, while other plans split the GPUs into several groups and process independent tasks in parallel. For example, if the calculation must be repeated for several coupling strengths, temperatures, disorder realizations, or random vectors, then different GPU groups may process different tasks at the same time.

To account for this, the benchmark score includes the number of task waves. Let $W(p)$ be the number of waves required to complete all independent tasks under plan p . For example, if there are N_{task} independent tasks and plan p can process $C(p)$ tasks at the same time, then

$$W(p) = \left\lceil \frac{N_{\text{task}}}{C(p)} \right\rceil.$$

Thus, $W(p) = 1$ means that all tasks can be processed in one wave, while $W(p) > 1$ means that the tasks must be processed in several consecutive batches.

The total benchmark score of plan p is defined as

$$S_{\text{bench}}(p) = W(p) \widehat{t}_{\text{mv}}(p). \quad (22)$$

Here:

- $S_{\text{bench}}(p)$ is the measured job-level score of plan p .
- $W(p)$ is the number of task waves required by plan p .
- $\widehat{t}_{\text{mv}}(p)$ is the measured average time for one matrix-free application under plan p .

A smaller value of $S_{\text{bench}}(p)$ means a better plan.

The measured autotuner does not test every possible plan. It only tests a small set of promising candidates selected by

the analytic planner. This set is denoted by $\mathcal{C}_{\text{bench}}$. The final measured plan is chosen as

$$p_{\text{bench}} = \arg \min_{p \in \mathcal{C}_{\text{bench}}} S_{\text{bench}}(p). \quad (23)$$

Here:

- $\mathcal{C}_{\text{bench}}$ is the set of candidate plans tested by the measured autotuner.
- p_{bench} is the plan with the lowest measured benchmark score.

In summary, the analytic planner first removes impossible or clearly poor plans. The measured autotuner then runs a small number of feasible plans on the actual hardware and selects the one with the best measured job-level runtime. This makes the final plan depend on real GPU performance rather than only on an approximate cost model.

The 18-qubit autotuning result in Fig. 1 gives a concrete example: plans with nearly identical single-kernel timings can differ at the job level because they require different numbers of GPU work waves.

a. Algorithm 2: measured autotuning. First run Algorithm 1 and retain the K_{bench} best feasible candidates. For each candidate, construct the same block source, cache mode, and GPU grouping that would be used in the production calculation. Apply the matrix-free operation several times, synchronizing the GPUs before and after the timed region. Record \widehat{t}_{mv} , memory metadata, GPU metadata, and the complete plan description. Choose the candidate minimizing Eq. (22).

D. Neural surrogate for community-scale plan selection

The third optimizer is a neural surrogate trained from accumulated benchmark records. Each measured trial produces a pair

$$(x(p), \widehat{t}_{\text{mv}}(p)),$$

where $x(p)$ is a numerical feature vector describing the problem, the plan, and the hardware. Typical features include

$$x(p) = (\log D_{\text{in}}, \log D_{\text{out}}, \log R, \log N_{\text{blk}}, \log b, \log N_{\text{task}}, p_{\text{row}}, \\ W(p), \mathbf{1}_{\text{full}}, \mathbf{1}_{\text{partial}}, \mathbf{1}_{\text{procedural}}, \mathbf{1}_{\text{g-parallel}}, \mathbf{1}_{\text{row}}, \mathbf{1}_{\text{hybrid}}, \\ \log F_{\text{mv}}, M_{\text{op}}/M_{\text{free}}, M_{\text{work}}/M_{\text{free}}, M_{\text{tot}}/M_{\text{free}}, \\ \text{GPU memory, GPU multiprocessors}).$$

The target is the logarithm of the measured time,

$$y(p) = \log \widehat{t}_{\text{mv}}(p).$$

The feature vector is normalized componentwise,

$$z = \frac{x - \mu}{\sigma},$$

and a one-hidden-layer surrogate is

$$f_{\theta}(x) = \tanh(zW_1 + b_1)W_2 + b_2, \quad (24)$$

where

$$\theta = \{W_1, b_1, W_2, b_2\}.$$

The predicted runtime is

$$\hat{t}_{\text{NN}}(p) = \exp(f_\theta(x(p))). \quad (25)$$

The network is trained by minimizing the log-time mean-squared error

$$\mathcal{L}(\theta) = \frac{1}{N} \sum_{i=1}^N [f_\theta(x_i) - \log \hat{t}_{\text{mv},i}]^2. \quad (26)$$

The logarithmic target is used because runtimes are positive and can vary by orders of magnitude. The hyperbolic tangent nonlinearity allows the surrogate to learn interactions between plan variables, such as the fact that a large row group is beneficial only for compatible cache layouts, or that memory pressure affects full-cache and procedural modes differently.

The neural surrogate is not used as an unchecked replacement for the physical or numerical model. It learns only the empirical hardware map

$$\text{problem} + \text{plan} + \text{hardware} \mapsto \text{runtime}.$$

In a hybrid planner, the neural model ranks many feasible candidates, and the measured autotuner benchmarks only the top K_{NN} candidates. Thus community and industry benchmark data can reduce the search cost on new machines while a local measurement remains the final decision rule.

a. Algorithm 3: learned and hybrid plan selection. Collect benchmark records from Algorithm 2 in a portable log containing hardware metadata, plan features, and measured matrix–multi-vector time. Train f_θ using Eq. (26). On a new machine, enumerate memory-feasible candidates with Algorithm 1, rank them by $\hat{t}_{\text{NN}}(p)W(p)$, and either choose the best neural candidate directly or benchmark the top K_{NN} candidates and select the best measured one using Eq. (23).

E. Adaptive block size

For equal block size b , one dense block requires

$$M_{\text{block}} = B_c b^2$$

bytes, where B_c is the number of bytes per complex number. Given a target single-block memory M_{target} , a natural block size is

$$b_{\text{target}} \approx \sqrt{\frac{M_{\text{target}}}{B_c}}.$$

The number of blocks can then be chosen so that

$$N_{\text{blk}} \gtrsim \frac{D}{b_{\text{target}}},$$

subject to divisibility, row-distribution requirements, and model-specific constraints. In power-of-two Hilbert spaces, choosing N_{blk} as a power of two is often convenient.

The block number should not be interpreted as a physical parameter. It is a memory-layout and scheduling parameter. If the procedural source is seeded, partition invariance requires that the generated matrix be independent of the chosen block partition. Otherwise different block counts correspond to different random samples and should not be compared as the same Hamiltonian.

F. Adaptive cache selection

Let $M_{\text{free}}^{(j)}$ be the free memory on GPU j . A cache budget can be chosen as

$$M_{\text{cache}} = f_{\text{cache}} \min_j M_{\text{free}}^{(j)},$$

where $0 < f_{\text{cache}} < 1$ is a safety fraction. If full caching of the Hamiltonian blocks fits within this budget, it is usually preferred for repeated Hamiltonian applications. If not, a partial cache can be used. For a Hermitian block matrix with equal block size, the number of canonical block pairs is

$$N_{\text{pair}} = \frac{N_{\text{blk}}(N_{\text{blk}} + 1)}{2}.$$

An approximate number of cached canonical pairs is

$$P_{\text{cache}} = \min \left[N_{\text{pair}}, \left\lfloor \frac{M_{\text{cache}}}{B_c b^2} \right\rfloor \right]. \quad (27)$$

The uncached pairs remain procedural or externally loaded. This creates a smooth transition between no caching and full caching.

Caching is most valuable when the same Hamiltonian is applied many times. Let R_H denote the approximate number of Hamiltonian–vector products in a run. For polynomial real-time propagation,

$$R_H \sim N_t p_{\text{rt}},$$

where N_t is the number of time samples and p_{rt} is the polynomial order. The measured growth of p_{rt} with Hilbert-space size in the 18-qubit series is shown in Fig. 3. More generally, let R_A denote the approximate number of times the same matrix or operator A is applied during a complete run. In repeated operator-application algorithms one may write schematically

$$R_A \sim \sum_{\ell} N_{\ell} p_{\ell},$$

where N_{ℓ} is the number of repetitions of stage ℓ , and p_{ℓ} is the number of matrix-vector applications required per repetition. The stages may represent time stepping, polynomial filtering, Krylov projection, iterative linear solvers, stochastic trace estimation, optimization iterations, sampling over random vectors, or repeated applications inside a machine-learning or scientific-computing pipeline.

When R_A is large, repeatedly regenerating or loading the same dense blocks can dominate runtime. In this regime, full GPU-resident caching, or row-distributed full caching, is strongly preferred whenever memory permits. Partial caching is useful only when the cached fraction is large enough to reduce repeated source access substantially.

G. Adaptive parallelization

Many quantum simulations include independent outer-loop parameters, such as coupling strengths, disorder realizations, temperatures and more. These can be distributed across GPUs without communication. We call this parameter-parallel execution.

For a single large Hamiltonian application, the work can instead be split by output block rows. If GPUs in a group are assigned disjoint row sets \mathcal{R}_j , GPU j computes

$$\phi^{[n]} = \sum_m \hat{H}^{[n,m]} \psi^{[m]}, \quad n \in \mathcal{R}_j.$$

This row-parallel strategy reduces per-GPU cached matrix memory because each GPU stores only the block rows it owns. A hybrid strategy combines parameter-parallelism between GPU groups with row-parallelism inside each group.

H. Dense-work safety estimates

For dense block graphs, matrix-free execution reduces matrix-storage pressure but does not remove dense arithmetic. A useful execution plan should therefore estimate the cost of one Hamiltonian application. For a dense $D \times D$ Hamiltonian, the leading work is proportional to

$$W_{H\psi} \sim O(D^2).$$

In a block implementation with equal block size b , the same estimate can be written as

$$W_{H\psi} \sim N_{\text{blk}}^2 O(b^2) = O(D^2).$$

If this estimate exceeds a user-defined threshold, the run can be rejected, warned, or forced explicitly. This prevents a memory-feasible but time-impractical dense calculation from being submitted accidentally.

For repeated-application algorithms, the more relevant estimate is

$$W_{\text{run}} \sim R_H W_{H\psi},$$

where R_H is the number of Hamiltonian applications implied by the propagator, filter, or correlation routine.

V. MEMORY AND RUNTIME SCALING

We now estimate the matrix memory footprint and runtime cost of the procedural block matrix-vector product. For clarity, assume equal block sizes,

$$b_n = b, \quad D = N_{\text{blk}} b.$$

Thus D is the full Hilbert-space dimension, N_{blk} is the number of vector blocks, and each block contains b complex entries.

A dense explicit Hamiltonian requires storage for a $D \times D$ complex matrix,

$$M_{\text{explicit}} = B_c D^2 = B_c N_{\text{blk}}^2 b^2, \quad (28)$$

where B_c is the number of bytes per complex number. This is the main memory barrier addressed by the framework.

The block representation does not change the mathematical size of a fully dense Hamiltonian. If all blocks $\hat{H}^{[n,m]}$ are stored at once on one device, then the matrix memory is still

$$M_{\text{blocks}} = B_c N_{\text{blk}}^2 b^2 = B_c D^2. \quad (29)$$

The advantage of the procedural method is that the full set of blocks does not need to be resident on a single GPU simultaneously. Blocks are generated, loaded, cached, distributed, or reconstructed only when their action is required.

Let q be the number of dense Hamiltonian blocks resident on a GPU at one time, with

$$1 \leq q \leq N_{\text{blk}}^2.$$

Then the active matrix memory on that GPU is

$$M_{\text{op,GPU}} = q B_c b^2. \quad (30)$$

The case $q = N_{\text{blk}}^2$ recovers full dense matrix storage on one GPU. The procedural case of interest is $q \ll N_{\text{blk}}^2$, where only a limited number of Hamiltonian blocks is materialized, applied, and then released. In row-distributed full caching, the full matrix is stored across a GPU group rather than on one device.

For a dense exact matrix-vector product, every output block receives contributions from every input block:

$$\phi^{[n]} = \sum_{m=0}^{N_{\text{blk}}-1} \hat{H}^{[n,m]} \psi^{[m]}. \quad (31)$$

The arithmetic cost remains

$$O(D^2).$$

The procedural method primarily reduces GPU-resident matrix memory. Runtime improvements occur when repeated source access is avoided by caching, when the block action is fused efficiently, when row distribution enables larger matrix-multiplication kernels, or when the Hamiltonian has exact block sparsity.

A. Runtime cost of procedural block access

Each block contribution has two costs: the cost of obtaining the block and the cost of applying it to the input vector block. Let $t_{\text{src}}(b)$ be the time required to obtain one $b \times b$ block, and let $t_{\text{mv}}(b)$ be the time required to multiply that block by a vector block. For the dense exact product,

$$N_{\text{blk}}^2$$

block pairs are included, so a simple runtime model is

$$T_{H\psi} \approx N_{\text{blk}}^2 [t_{\text{src}}(b) + t_{\text{mv}}(b)] \quad (32)$$

when source access and computation are not overlapped. If block access and computation are overlapped by asynchronous execution or double buffering, the block-pair time is closer to

$$T_{H\psi} \approx N_{\text{blk}}^2 \max [t_{\text{src}}(b), t_{\text{mv}}(b)]. \quad (33)$$

Thus, the calculation can be compute-limited, source-limited, or transfer-limited depending on how the blocks are obtained.

A dense $b \times b$ block contains b^2 complex entries, so its size is

$$S_{\text{block}} = B_c b^2. \quad (34)$$

a. Externally stored blocks. If a block is loaded from file, host memory, a database, or another external storage layer, then the source time per block is approximately

$$t_{\text{src}}^{\text{ext}}(b) \approx t_{\text{lat}} + \frac{B_c b^2}{\mathcal{B}_{\text{eff}}}. \quad (35)$$

Here t_{lat} is the per-block latency or lookup overhead, and \mathcal{B}_{eff} is the effective bandwidth from the source to GPU-usable memory.

b. Seeded generation. If a block is generated from a seed, the transferred metadata may be much smaller than the dense block itself. Let S_{seed} be the metadata size per block and let R_{gen} be the effective rate for generating Hamiltonian entries. Then

$$t_{\text{src}}^{\text{seed}}(b) \approx t_{\text{lat}} + \frac{S_{\text{seed}}}{\mathcal{B}_{\text{meta}}} + \frac{b^2}{R_{\text{gen}}}. \quad (36)$$

Seeded generation reduces storage and data movement because only compact metadata must be retained. The cost is that the matrix entries must be regenerated unless the block is cached.

Seeded generation is most attractive when the block is used only a small number of times, when generation is fused with the contraction, or when memory is insufficient for caching. It is less attractive when the same block is needed in many Hamiltonian applications. In repeated propagation or TPQ filtering, repeated seeded generation can become a dominant cost unless it is overlapped with computation or replaced by caching.

c. Analytic generation. If a block is defined by an analytic formula

$$\hat{H}_{\alpha\beta}^{[n,m]} = f(n, m, \alpha, \beta; \theta),$$

then the source time depends on the cost of evaluating f . If R_{ana} is the effective rate for evaluating analytic matrix entries, then

$$t_{\text{src}}^{\text{ana}}(b) \approx \frac{b^2}{R_{\text{ana}}}. \quad (37)$$

d. Cached blocks. For cached blocks, the source cost is replaced by cache-access cost. If the cache is GPU-resident, $t_{\text{src}}(b)$ can be much smaller than regeneration or external loading. The price is persistent memory use. Partial caching makes t_{src} block dependent:

$$t_{\text{src}}(n, m) = \begin{cases} t_{\text{cache}}, & (n, m) \in \mathcal{P}_{\text{cache}}, \\ t_{\text{regen/load}}, & (n, m) \notin \mathcal{P}_{\text{cache}}. \end{cases}$$

For dense repeated-application workloads, the preferred storage hierarchy is

single-GPU full cache \rightarrow row-distributed full cache
 \rightarrow partial cache \rightarrow procedural or external streaming.

The first two regimes preserve reuse of matrix data. Partial caching reduces memory but may still require repeated generation or loading of uncached blocks. Procedural generation minimizes memory but can be much slower when the same Hamiltonian is applied many times.

B. Selected block graphs

A secondary case occurs when only a subset of block products is included. This may happen for an exactly block-sparse Hamiltonian, a controlled truncation, or a stochastic sampling scheme. If each output block is coupled to only z input blocks on average, with $z \ll N_{\text{blk}}$, then

$$\phi^{[n]} = \sum_{m \in \mathcal{N}(n)} \hat{H}^{[n,m]} \psi^{[m]}, \quad |\mathcal{N}(n)| \approx z. \quad (38)$$

The number of block products is then zN_{blk} instead of N_{blk}^2 . This reduction is exact only if the omitted blocks are truly zero. If blocks are omitted by truncation or sampling, the result is an approximate or stochastic matrix-vector product.

VI. GPU-RESIDENT MATRIX CACHING AND ROW DISTRIBUTION

The most efficient regime for repeated dense Hamiltonian application is to keep reusable matrix data on the GPU. If the complete dense Hamiltonian cache fits on one device, the implementation can apply the matrix with large dense matrix-vector or matrix-matrix kernels. If the cache does not fit on one GPU but does fit across a group of GPUs, the matrix can be distributed by output rows.

In row-distributed full caching, a GPU group of size p_{row} stores disjoint row slices of the dense Hamiltonian. GPU j stores

$$H_{\text{local}}^{(j)} \in \mathbb{C}^{D_j \times D},$$

where $D_j \approx D/p_{\text{row}}$. The per-GPU matrix memory is approximately

$$M_{\text{local}} \approx \frac{B_c D^2}{p_{\text{row}}}.$$

Each GPU computes its local output segment,

$$\phi^{(j)} = H_{\text{local}}^{(j)} \psi.$$

The local outputs can then be gathered or kept distributed for subsequent kernels.

This strategy is useful because the communication volume associated with a Hamiltonian application is linear in D , while the dense arithmetic is quadratic in D . For sufficiently large dense matrices, the computation can therefore remain dominated by local dense linear algebra rather than by the cost of communicating the vector. The preferred data layout stores

Method	GPU-resident matrix memory	Main runtime contribution
Explicit dense global \hat{H}	$O(D^2)$	Dense matrix-vector product after the matrix is resident
Procedural dense matrix, all block pairs included	$O(qb^2)$, with $1 \leq q \leq N_{\text{blk}}^2$	$N_{\text{blk}}^2 [t_{\text{src}}(b) + t_{\text{mv}}(b)]$, or the overlapped maximum
Partially cached block matrix	$O(p_{\text{cache}}b^2)$ plus active workspace	Cached blocks use t_{cache} ; uncached blocks use regeneration or loading
Row-distributed full cache	Approximately $O(D^2/p_{\text{row}})$ per GPU	Dense row-slice products plus row communication
Selected block graph with z input neighbors per output block	$O(qb^2)$, with $q \leq zN_{\text{blk}}$	$zN_{\text{blk}} [t_{\text{src}}(b) + t_{\text{mv}}(b)]$

TABLE I. Scaling regimes for $D = N_{\text{blk}}b$. The dense procedural case includes all N_{blk}^2 block products and primarily reduces GPU-resident matrix memory. Caching changes the source cost but uses persistent memory. Sparse, truncated, or sampled block graphs reduce the number of block products only when their assumptions are valid.

each local row slice contiguously so that the dominant operation is a large GEMM(General Matrix Matrix Multiplication)-like kernel rather than a long sequence of small block contractions.

Host memory or external storage can be useful as a staging layer, but using it as the active source for every Hamiltonian application is usually unfavorable when the same Hamiltonian is applied many times. If matrix data of size M_{op} are streamed from host to GPU for every Hamiltonian-vector product, the total data movement scales as

$$R_H M_{\text{op}},$$

where R_H is the number of Hamiltonian applications. For polynomial propagation, TPQ filtering, and correlation calculations, R_H can be very large. In such cases, host-resident matrix data should be transferred to the GPU once when possible, or used to build a GPU-resident cache. Streaming from host memory in the inner loop is mainly a fallback for cases where no GPU-resident representation is feasible.

A practical adaptive implementation therefore attempts the following sequence:

1. use a single-GPU full cache when the dense matrix fits on one GPU;
2. use row-distributed full caching when the dense matrix fits across a GPU group;
3. use partial caching when full caching is impossible but a large reusable fraction fits;
4. use procedural generation or external streaming only when caching is not feasible.

This hierarchy is not a physical approximation. It is a storage and scheduling hierarchy for the same mathematical Hamiltonian.

VII. EXAMPLE: AUTOTUNED PROPAGATION OF AN 18-QUBIT STATE ON PARALLEL GPUS

The example consists of a real-time evolution, of the state ψ governed by the Schrödinger equation:

$$i \frac{d}{dt} \psi(t) = \hat{H} \psi(t), \quad (39)$$

with formal solution

$$\psi(t + \Delta t) = e^{-i\Delta t \hat{H}} \psi(t). \quad (40)$$

We illustrate the current implementation with a concrete run produced by ADGOM.py. (List VII) The example uses the same Hamiltonian action as above, but the execution plan is not fixed by hand. The code first constructs a dense-matvec planning problem, rejects memory-infeasible candidates, benchmarks the remaining candidates on the allocated GPUs, and then uses the measured fastest plan for the TPQ and correlation calculation.

The simulated Hilbert space contains two system qubits and sixteen bath qubits,

$$d_S = 2^2 = 4, \quad d_B = 2^{16} = 65536.$$

The total Hilbert-space dimension is therefore

$$D = d_S d_B = 2^{18} = 262144.$$

A state vector has D complex amplitudes. This vector can still be stored on modern GPUs in single or double precision. The dense Hamiltonian, however, would require storage for a $D \times D$ complex matrix. For complex64 arithmetic this is approximately

$$8D^2 = 8(2^{18})^2 = 2^{39} \text{ bytes} \approx 512 \text{ GiB},$$

and for complex128 arithmetic it is approximately 1 TiB. Thus the state vector is not the memory bottleneck; explicit storage of the full system-bath Hamiltonian is.

The Hamiltonian used in the code has the form

$$\hat{H} = H_S \otimes I_B + I_S \otimes H_B + g \sum_{a=1}^{N_{\text{int}}} A_a \otimes B_a,$$

where H_B and the B_a are dense bath-space operators represented in bath blocks. The action of the Hamiltonian on a state

$$\psi \in \mathbb{C}^{d_S} \otimes \mathbb{C}^{d_B}$$

is evaluated without constructing the full $D \times D$ Hamiltonian. In block form, the dominant bath-side operation is

$$\phi^{[n]} = \sum_{m=0}^{N_{\text{blk}}-1} H_B^{[n,m]} \psi^{[m]},$$

together with the analogous block actions for the interaction operators B_a .

The run used one interaction bath operator, so each Hamiltonian application uses two dense bath-side operators, H_B and B_1 . In complex64 arithmetic, one full bath-side operator has size

$$8d_B^2 = 8(65536)^2 = 32 \text{ GiB}.$$

The two bath-side operators therefore require 64 GiB if stored on a single GPU. This exceeds the memory of one L40S GPU, but fits when the operator rows are distributed over pairs of GPUs. The autotuner selected

$$N_{\text{blk}} = 16, \quad b = \frac{d_B}{N_{\text{blk}}} = 4096,$$

so one complex64 block occupies $4096^2 \times 8 = 128 \text{ MiB}$. Each GPU in a two-GPU row group stores a contiguous local slice of shape

$$32768 \times 65536$$

for each bath-side operator, corresponding to 16 GiB per operator and 32 GiB per GPU for the two operators.

The propagation is performed by repeated matrix-free Hamiltonian applications. The code uses a centered Chebyshev propagation³. First, matrix-free Lanczos iterations estimate spectral bounds E_{\min} and E_{\max} . The Hamiltonian is then scaled as

$$\tilde{H} = \frac{\hat{H} - cI}{R}, \quad c = \frac{E_{\max} + E_{\min}}{2}, \quad R = \frac{E_{\max} - E_{\min}}{2}.$$

The Chebyshev recurrence is

$$q_0 = \psi, \tag{41}$$

$$q_1 = \tilde{H}q_0, \tag{42}$$

$$q_{\ell+1} = 2\tilde{H}q_{\ell} - q_{\ell-1}. \tag{43}$$

In block form this becomes

$$q_{\ell+1}^{[n]} = 2 \sum_{m=0}^{N_{\text{blk}}-1} \tilde{H}^{[n,m]} q_{\ell}^{[m]} - q_{\ell-1}^{[n]}. \tag{44}$$

The numerical intensive operation in the recurrence is the repeated application of \tilde{H} , which is precisely the matrix-free block operation described above.

The calculation was run on a single SLURM node with eight NVIDIA L40S GPUs. Each GPU reported 44.39 GiB total memory, 43.97 GiB free memory at job start, 142 streaming multiprocessors, and CUDA compute capability 8.9. The submission script requested eight L40S GPUs, four CPU cores, and 64 GB of host memory, loaded CUDA 12.8.1 when available, and used a lab-local CuPy kernel cache.

The initial autotuning submission, using ADGOM.py (adaptive_dense_gpu_optimized_matvec.py), was:

List VII:

```
[basicstyle=\ttfamily\scriptsize,
  aboveskip=4pt,
  belowskip=4pt]
python -u adaptive_dense_gpu_optimized_matvec.py \
  --num-gpus 8 \
  --log2-sys 2 \
  --log2-bath-list 16 \
  --seed 3 \
  --num-g 20 \
  --max-g-factor 1.0 \
  --beta 0.2 \
  --eps-list 0.1 \
  --K-hmf 50 \
  --K-corr 1 \
  --num-int-ops 1 \
  --n-blocks auto \
  --operator-mode auto \
  --parallel-mode auto \
  --row-group-size auto \
  --planner-mode autotune \
  --autotune-repeats 3 \
  --autotune-warmup 1 \
  --autotune-max-candidates 8 \
  --plan-trial-log q18_bath16_plan_trials.jsonl \
  --sampling-source bare \
  --sampling-spacing-floor 0 \
  --sampling-max-N 200 \
  --dtype complex64 \
  --cheb-tol 1e-7 \
  --lanczos-m 40 \
  --skip-exact-rdm \
  --no-diagnostics \
  --checkpoint-dir q18_bath16_auto_checkpoints
```

The measured planner benchmarked eight candidate plans. The selected plan was full-cache hybrid execution with row-group size 2:

$$\text{gpu groups} = [[0, 1], [2, 3], [4, 5], [6, 7]].$$

The selected plan used $N_{\text{blk}} = 16$, $b = 4096$, full-cache storage, and complex64 arithmetic. The planner estimated 32 GiB of operator storage per GPU, 116 MiB of state/workspace memory per primary GPU, and 32.1 GiB total memory per GPU. The estimated work per Hamiltonian application was

$$2d_S d_B^2 8 = 2.749 \times 10^{11}$$

real floating-point operations. The measured microbenchmark time was 0.104089 s per $\tilde{H}\psi$ application for the selected plan. The effective planner score was 0.520447 s, corresponding to five waves of work for 20 coupling values over four GPU groups.

The measured autotuning outcome is shown in Fig. 1. The best few feasible plans are very close in raw $\tilde{H}\psi$ time, so the

planner decision is not determined by a single kernel timing alone. The relevant quantity is the measured kernel time multiplied by the number of GPU work waves required to cover all coupling values.

The physical and numerical parameters were

$$\beta = 0.2, \quad K_{\text{HMF}} = 50, \quad K_{\text{corr}} = 1, \quad N = 200, \\ \tau = 0.1982748544807706.$$

The coupling grid contained 20 values from $g = 0$ to $g_{\text{max}} = 6.3378539$. The bare-system sampling rule selected

$$T = N\tau = 39.654971, \quad \pi/\tau = 15.844635.$$

For the completed checkpointed trajectories, matrix-free Lanczos gave spectral radii near 713. The imaginary-time TPQ Chebyshev filter used order 80, and the centered real-time Chebyshev propagator used order 181 per time step. The dependence of this Chebyshev order on Hilbert-space dimension is shown in Fig. 3.

The calculation was completed in two checkpointed SLURM submissions. The initial autotuning job selected the plan above and wrote checkpoints for the fifteen zero-based coupling indices 5, ..., 19. The checkpoint continuation then reused the same directory, `q18_bath16_auto_checkpoints`, and specified the selected plan directly,

```
full-cache, hybrid, row-group-size=2, N_blk=16,
```

without repeating the autotuning benchmark. This continuation completed the missing zero-based indices 0, ..., 4, so the checkpoint directory now contains

```
gidx_0000.npz, ..., gidx_0019.npz.
```

The continuation job finished in 6258.74 s and assembled the final output file

```
wave_adaptive_dense_tpq_raw_modefull-cache
_parhybrid_KHMF50_KC1_nint1_2_16_N200
_tau0p198274854481_nb16.npz.
```

Figures 2 and 3 summarize the computational scaling observed in the same two-system-qubit series. The end-to-end runtime reports the time needed to produce a completed result file, while the Chebyshev order reports the number of Hamiltonian applications required for one real-time step.

The saved arrays had shapes

$$\text{corr_per_g_eps} = (20, 1, 200), \quad \text{C_per_tpq} = (20, 1, 1, 200).$$

Excluding the non coupling case across all nineteen coupling values, the measured propagation times were tightly clustered between 3745.79 s and 3754.00 s, with mean 3749.84 s. The resulting end-to-end runtime scaling is summarized in Fig. 2. This example demonstrates the practical role of the method. The dense Hamiltonian action is not made cheap: the calculation remains a large dense matrix-free propagation. The advantage is that the execution plan is chosen on the target

hardware and the calculation is no longer blocked by the requirement to assemble or store the full $2^{18} \times 2^{18}$ Hamiltonian on one GPU. The memory requirement is converted into a combination of full GPU-resident row caches, state/workspace buffers, checkpointing, and measured GPU grouping.

VIII. LIMITATIONS AND DESIGN IMPLICATIONS

The framework changes matrix memory scaling and scheduling, but it does not make a fully dense Hamiltonian cheap. If all block pairs are nonzero, the exact Hamiltonian-vector product still has dense arithmetic cost. In such a case, the method can make the calculation possible from the standpoint of matrix storage, but the remaining runtime may still be impractical. This separation between memory feasibility and runtime cost is visible in Fig. 2, where the calculation becomes possible but the completed-result time still grows rapidly with Hilbert-space size.

This limitation leads to several design implications. First, caching is useful only when the cached data are reused. Repeated propagation and TPQ filtering are favorable because they apply the same Hamiltonian many times. Second, partial caching is not automatically efficient. If a large fraction of the matrix must still be regenerated or loaded at every Hamiltonian application, partial caching can be much slower than full caching. Third, row-distributed full caching is preferable when the full dense matrix does not fit on one GPU but does fit across a GPU group. Fourth, streaming matrix data from CPU memory in the inner loop should be treated as a fallback, not as the preferred regime, when the Hamiltonian is applied many times.

Fifth, optimization of the execution plan should be interpreted as empirical performance modeling, not as a physical approximation. The analytic planner rejects memory-infeasible candidates and ranks feasible candidates by a cost model. The measured autotuner replaces that ranking by direct timings on the target hardware. The neural surrogate learns only the hardware-dependent map from problem features and plan features to runtime. It should therefore be used as a ranking prior, or as part of a hybrid planner followed by local measurement, unless it has been validated on the relevant hardware class and problem family.

The block partition should also be designed carefully. Too few blocks can make single-block memory too large and prevent row distribution. Too many blocks can increase overhead and reduce arithmetic intensity. In dense row-distributed execution, the best implementation stores local row slices as contiguous matrices and applies them with large GEMM-like kernels. The mathematical block partition remains general, but the data layout strongly affects performance.

Finally, computational parameters must be separated from the Hamiltonian being simulated. The block count, block size, cache mode, GPU grouping, and row-group size are execution choices. They should not change the Hamiltonian. If a procedural source depends on the block partition, then these execution choices become part of the random sample and must be reported and validated. A partition-invariant source avoids

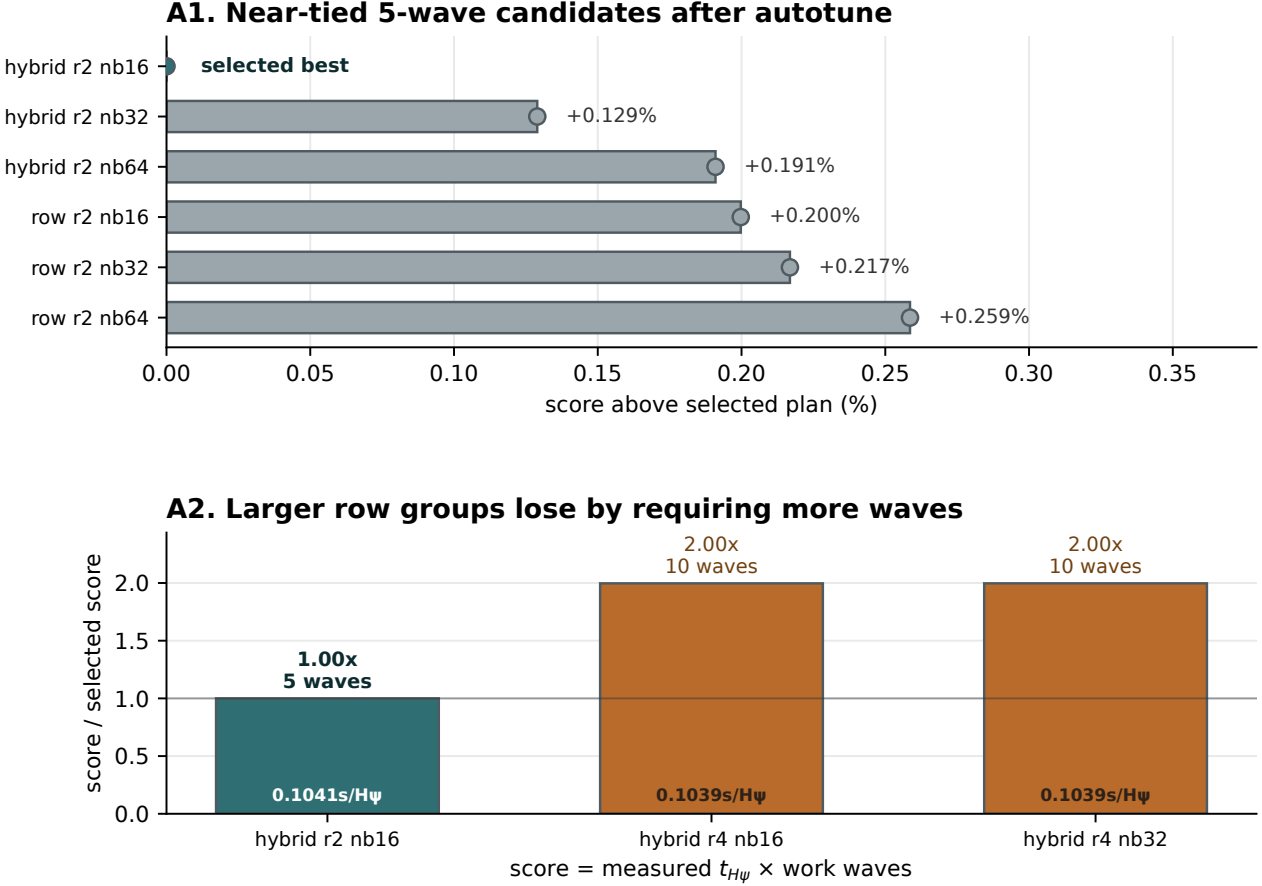


FIG. 1. Measured autotuning of the 18-qubit execution plan on eight NVIDIA L40S GPUs. A1 shows the near-tied five-wave candidates after the autotune stage, plotted as the score increase relative to the selected plan. The selected full-cache hybrid plan with row-group size 2 and $N_{\text{blk}} = 16$ is only marginally faster than several alternatives, but it has the lowest measured score. A2 separates the reason that some apparently competitive candidates are rejected: plans with row-group size 4 have nearly the same measured $\hat{H}\psi$ time, but they require ten GPU work waves rather than five. The autotuner therefore chooses the plan that minimizes total scheduled work, not merely the plan with the smallest single-application timing.

this problem by defining matrix entries from global indices rather than from block labels.

IX. DISCUSSION

The framework presented here is motivated by a simple principle: in large quantum simulations, the mathematical Hilbert space may be fixed by the physics, but the memory representation of the Hamiltonian matrix is an algorithmic choice. Explicitly storing the full Hamiltonian on one GPU should not be the only route to exact or controlled quantum-state propagation.

The method separates the mathematical Hamiltonian from its storage. The operator \hat{H} remains a single well-defined block matrix, but its entries are supplied procedurally and only when required by the current computation. This makes it possible to apply Hamiltonians whose full dense representation would exceed single-GPU memory. In this sense, the framework turns the size of the matrix from a hard storage constraint into

a scheduling, generation, caching, data-layout, and bandwidth problem.

The block representation in Eq. (3) is mathematically general: any finite matrix can be partitioned into blocks. Its computational value comes from how those blocks are generated, loaded, compressed, fused, cached, distributed, or scheduled. For a fully dense block matrix, the method primarily reduces GPU memory requirements rather than arithmetic complexity. If the block graph is sparse, so that only $m \in \mathcal{N}(n)$ contribute to each output block, then the product becomes

$$\phi^{[n]} = \sum_{m \in \mathcal{N}(n)} \hat{H}^{[n,m]} \psi^{[m]},$$

which can reduce both memory traffic and arithmetic cost. The direct-sum case is the limiting situation $\mathcal{N}(n) = \{n\}$.

Hardware adaptiveness is not a separate physical approximation. It is an execution strategy for the same mathematical operation. A large-memory GPU may prefer full caching; a smaller GPU may require row-distributed full caching, partial caching, or procedural generation; a parameter scan may

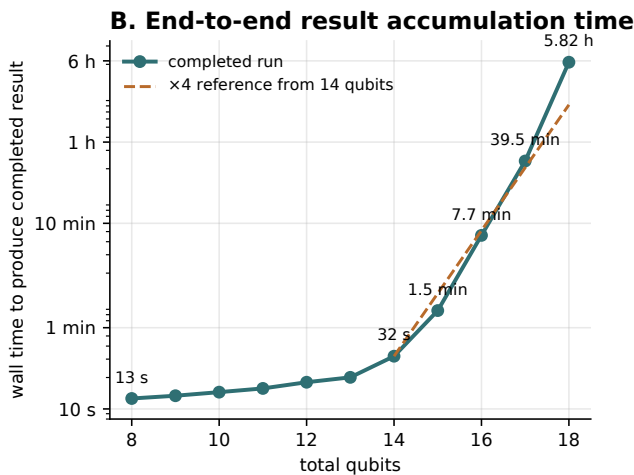


FIG. 2. End-to-end accumulation time for the completed two-system-qubit calculations. Each point is a completed run with $N = 200$ time samples, $K_{\text{HMF}} = 50$, $K_{\text{corr}} = 1$, one interaction bath operator, and complex64 arithmetic. The dashed line is a reference $4\times$ growth per added bath qubit, anchored at the 14-qubit result where the dense bath-side work begins to dominate. The measured curve shows the practical cost of producing the saved result files, including propagation, scheduling, checkpoint handling when used, and final assembly.

prefer independent GPU workers; a single large calculation may prefer row-parallel execution. The optimal strategy is therefore not universal. It depends on the relationship between matrix size, cache budget, bandwidth, data layout, and arithmetic throughput. The measured plan comparison in Fig. 1 is an example of this hardware dependence: the selected plan is determined by the combination of memory feasibility, kernel timing, and available GPU concurrency. The analytic, measured, and learned planners make this dependency explicit. The analytic planner gives a reproducible memory-feasible baseline; the measured autotuner adapts the baseline to the actual accelerator, driver, interconnect, and kernel implementation; and the neural surrogate provides a way to reuse benchmark experience across machines. Because the feature vector is defined for the generic dense matrix–multi-vector product, the same planner can be applied to the kicked TPQ/HMF model, to other Hamiltonian families, and to non-Hamiltonian large linear maps. For example the Liouvillian generator \mathcal{L} in open quantum systems^{18,19}.

This data-driven layer also suggests a useful community and industrial workflow. Each benchmark record contains the mathematical problem size, the candidate execution plan, hardware metadata, and the measured matrix–multi-vector time. Such records do not reveal the full scientific dataset or proprietary matrix entries; they describe how fast a declared linear-algebra operation ran under a declared plan. Aggregating these records would allow the neural surrogate to improve as more laboratories, clusters, and industrial deployments contribute timings.

This distinction is especially important when the matrix is generated procedurally. Cache mode should not change the Hamiltonian, but the generation rule can accidentally make the block partition part of the random sample. For physical com-

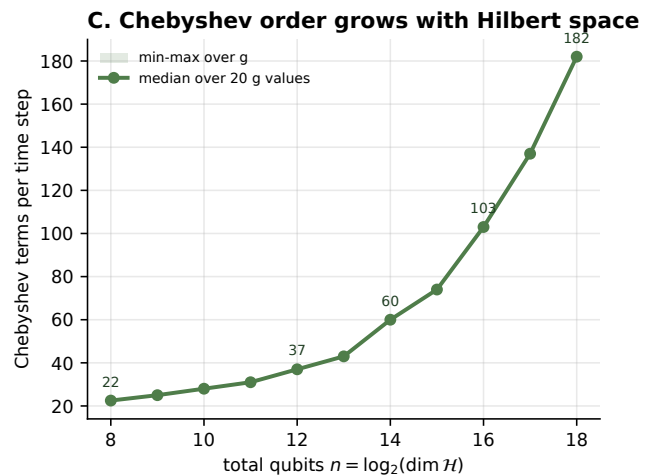


FIG. 3. Real-time Chebyshev order as a function of Hilbert-space size for the same completed two-system-qubit calculations. For each total qubit count, the order was computed from the saved Lanczos half-widths R , the selected time step τ , and the same coefficient-tolerance rule used by the propagation code. Points show the median over the twenty coupling values, and the shaded band shows the corresponding minimum–maximum range. The increase from about 23 terms at 2^8 dimension to about 182 terms at 2^{18} demonstrates that the larger simulations are more expensive not only because the vectors and block operations are larger, but also because each physical time step requires more Chebyshev Hamiltonian applications.

parisons at fixed disorder realization or fixed random matrix sample, the procedural generator must be partition invariant.

The method is most advantageous when the cost of generating or loading a block is small compared with the cost of storing the global matrix, when cached blocks are reused many times, when the block action can be fused with the contraction, when row-distributed caching enables large local GEMM operations, or when the same Hamiltonian is applied repeatedly. Propagation, TPQ filtering, and correlation calculations all have this repeated-application structure, so implementation effort spent on the matrix-free kernel and adaptive execution plan is amortized over many Hamiltonian applications.

The general approach can also be adopted to quantum computing using the idea of Block-encoding and unitary matrix dilation²⁰.

X. CONCLUSION

We have presented a procedural matrix-free and hardware-adaptive framework for applying very large Hamiltonians on GPUs without storing the full dense matrix on a single device. The Hamiltonian is treated as one block-partitioned operator,

$$\hat{H} = \left(\hat{H}^{[n,m]} \right)_{n,m=0}^{N_{\text{blk}}-1},$$

and the matrix-vector product is evaluated by the blockwise rule

$$\phi^{[n]} = \sum_{m=0}^{N_{\text{blk}}-1} \hat{H}^{[n,m]} \psi^{[m]}.$$

The global $D \times D$ Hamiltonian is never assembled on a single device. Matrix blocks are generated, loaded, cached, distributed, or reconstructed only when needed.

The main contribution is a memory-scalable architecture for Hamiltonian application together with an adaptive execution strategy. For a fully dense Hamiltonian, the arithmetic cost of the exact matrix-vector product is not removed. However, the GPU-resident matrix-memory requirement is changed fundamentally: instead of requiring the full Hamiltonian on one GPU, the computation can require only selected blocks, cached data, row-distributed matrix slices, and temporary workspace. This allows simulations to be attempted in regimes where explicit Hamiltonian storage would otherwise be impossible.

We have also formulated execution planning itself as a general dense matrix-multi-vector optimization problem. In this formulation, the planner chooses among mathematically equivalent implementations of $Y = AX$. The paper describes three plan-selection algorithms: a memory-constrained analytic cost-model planner, a measured microbenchmark autotuner, and a neural surrogate trained from logged trials. The learned model does not alter the operator or the numerical method; it predicts which feasible execution plan is likely to run fastest, and in the hybrid mode it reduces the number of local benchmarks needed before the final measured choice is made.

The same matrix-application kernel supports quantum real-time propagation, imaginary-time filtering, stochastic TPQ preparation, observable estimation, and correlation-function evaluation²¹. In each of these cases, the essential computational task is the repeated application of a large linear operator to one or more vectors. Beyond quantum simulation, the same structure appears in many algorithms dominated by large linear maps. This includes scientific machine learning and artificial-intelligence workloads, where matrix-vector or matrix-matrix operations appear in linear layers, projection operators, embedding maps, attention mechanisms, kernel methods, iterative optimization, and large-scale inference²².

The procedural interface used here is therefore not tied to Hamiltonian dynamics alone. Hamiltonian-vector multiplication is a prominent quantum-mechanical example of a broader class of memory-limited operator-vector and matrix-vector multiplication problems. Within this broader view, seeded random blocks, analytic formulas, fused block actions, cached blocks, and externally stored deterministic matrix data are simply different ways of supplying the local pieces of a large linear map without explicitly materializing the full matrix on a single device.

As exact and controlled quantum simulations become increasingly important for benchmarking quantum computers and developing quantum technologies, matrix memory scalability becomes a central requirement. The framework developed here provides a route toward simulations in which available GPU memory is no longer identified only with the ability to

store the full Hamiltonian matrix. The remaining limits become explicit and tunable: block generation, caching, data movement, parallel scheduling, arithmetic throughput, and algorithmic accuracy.

ACKNOWLEDGMENTS

We thank Raam Uzdin for support and useful discussion. We acknowledge the support of the Hebrew University Research Computing Services (HURCS) for hosting this study and The Fritz Haber center for overall support.

- ¹H. De Raedt, J. Kraus, A. Hertel, V. Mehta, M. Bode, M. Hrynnyak, K. Michielsen, and T. Lippert, "Universal quantum computer simulation of 50 qubits on europe's first exascale supercomputer harnessing its heterogeneous cpu-gpu architecture," *Future Generation Computer Systems*, 108592 (2026).
- ²R. Kosloff, "Propagation methods for quantum molecular dynamics," *Annual review of physical chemistry* **45**, 145–178 (1994).
- ³H. Tal-Ezer and R. Kosloff, "An accurate and efficient scheme for propagating the time dependent schrödinger equation," *The Journal of chemical physics* **81**, 3967–3971 (1984).
- ⁴R. Kosloff and H. Tal-Ezer, "A direct relaxation method for calculating eigenfunctions and eigenvalues of the schrödinger equation on a grid," *Chemical Physics Letters* **127**, 223–230 (1986).
- ⁵M. R. Wall and D. Neuhauser, "Extraction, through filter-diagonalization, of general quantum eigenvalues or classical normal mode frequencies from a small number of residues or a short-time segment of a signal. i. theory and application to a quantum-dynamics model," *The Journal of chemical physics* **102**, 8011–8022 (1995).
- ⁶R. Baer and M. Head-Gordon, "Chebyshev expansion methods for electronic structure calculations on large molecular systems," *The Journal of chemical physics* **107**, 10003–10013 (1997).
- ⁷J. Eckseler, M. Pieper, and J. Schnack, "Escaping the krylov space during the finite-precision lanczos algorithm," *Physical Review E* **112**, 025306 (2025).
- ⁸A. Braun and P. Schmitteckert, "Numerical evaluation of green's functions based on the chebyshev expansion," *Physical Review B* **90**, 165112 (2014).
- ⁹Y. Saad and M. H. Schultz, "Gmres: A generalized minimal residual algorithm for solving nonsymmetric linear systems," *SIAM Journal on scientific and statistical computing* **7**, 856–869 (1986).
- ¹⁰T. Westerhout and B. L. Chamberlain, "Implementing scalable matrix-vector products for the exact diagonalization methods in quantum many-body physics," in *Proceedings of the SC'23 Workshops of the International Conference on High Performance Computing, Network, Storage, and Analysis* (2023) pp. 1140–1150.
- ¹¹Y. Saad, "Numerical solution of large nonsymmetric eigenvalue problems," *Computer Physics Communications* **53**, 71–90 (1989).
- ¹²H. De Raedt, "Product formula algorithms for solving the time dependent schrödinger equation," *Computer Physics Reports* **7**, 1–72 (1987).
- ¹³A. Dax, "A new type of restarted krylov methods," *Adv. Linear Algebra Matrix Theory* **7**, 18–28 (2017).
- ¹⁴J. Baglama and L. Reichel, "Augmented implicitly restarted lanczos bidiagonalization methods," *SIAM Journal on Scientific Computing* **27**, 19–42 (2005).
- ¹⁵B. Charlier, J. Feydy, J. A. Glaunes, F.-D. Collin, and G. Durif, "Kernel operations on the gpu, with autodiff, without memory overflows," *Journal of Machine Learning Research* **22**, 1–6 (2021).
- ¹⁶A. Wietek and A. M. Läuchli, "Sublattice coding algorithm and distributed memory parallelization for large-scale exact diagonalizations of quantum many-body systems," *Physical Review E* **98**, 033309 (2018).
- ¹⁷S. Sugiura and A. Shimizu, "Canonical thermal pure quantum state," *arXiv preprint arXiv:1302.3138* (2013).
- ¹⁸R. Kosloff, "Quantum thermodynamics and open-systems modeling," *The Journal of chemical physics* **150** (2019).
- ¹⁹P. Zhao, H. De Raedt, S. Miyashita, F. Jin, and K. Michielsen, "Dynamics of open quantum spin systems: An assessment of the quantum master equation approach," *Phys. Rev. E* **94**, 022126 (2016).

- ²⁰K. J. Joven, E. R. Das, J. Bierman, A. Majumdar, M. H. Heris, and Y. Liu, “Scalable quantum computational science: A perspective from block-encodings and polynomial transformations,” *APL Computational Physics* **2** (2026).
- ²¹H. Endo, C. Hotta, and A. Shimizu, “From linear to nonlinear responses of thermal pure quantum states,” *Physical review letters* **121**, 220601 (2018).
- ²²T. Dao, D. Y. Fu, S. Ermon, A. Rudra, and C. Ré, “Flashattention: Fast and memory-efficient exact attention with io-awareness,” in *Advances in Neural Information Processing Systems*, Vol. 35 (2022) pp. 16344–16359.